Appendix A Geochronology

A1 Rb-Sr Methods and Sample Descriptions

Cm-sized pieces of rock were cut out from hand samples to isolate specific fabrics corresponding to progressive stages of deformation-metamorphism as outlined in Section 4. Samples were crushed with a small hammer between sheets of paper, and ground gently with a mini metal rock crusher to separate mineral aggregates. Samples were sieved and separated by grain size. Grain size fractions 125-250 μm and 250-500μm were frantzed to separate minerals based on magnetic susceptibility. The first pass was done with strongest magnetic setting (~1.8 Amperes) to remove all non-magnetics (e.g. quartz). Subsequent passes were done starting at the lowest setting where minerals started to magnetically separate (typically ~0.2-0.4 A); separates were repeatedly passed through the Frantz at increments of ~0.1-0.2 A. Magnetic fractions were then cleaned by hand, by either negative or positive picking of phases of interest, including garnet, glaucophane, epidote, and white micas (and apatite and chlorite for retrograde fabrics). White mica separates were cleaned of inclusions by gently smearing them in a mortar and pestle and washing them through a sieve with ethanol.

SY1616 was collected from float blocks at Kini Beach immediately beneath in-place blueschist-to-eclogite facies cliff faces. The sample is representative of D_S in blueschist-eclogite lithologies. The foliation is defined by glaucophane, epidote, phengite, paragonite, and rutile, with porphyroblasts of garnet and omphacite. Glaucophane, epidote, omphacite, and phengite define the lineation. A similar rock type is shown in Figure 7A. The prograde fabric was targeted for geochronology.

KCS1617 was collected from Azolimnos (approximate location: 37° 24'43.86"N, 24° 57'55.42"E). The sample records an older D_S cleavage cross-cut by the D_{T1} upright crenulation. The mineral assemblage includes glaucophane, epidote, quartz, phengite, paragonite, garnet, rutile, titanite, and oxides. The D_{T1} fabric was cut out of the sample using a diamond-tipped rock saw and targeted for geochronology.

KCS1621 was collected from the southern side of Delfini Beach (approximate location: 37°27'14.61"N, 24°53'51.23"E). The sample is representative of D_{T2}. The foliation is defined by quartz, phengite, paragonite and the lineation is defined by porphyroblasts of epidote and actinolite. This sample is interbedded with quartz-rich schists that have a blue amphibole lineation decimeters to meters above and below. The greenschist-facies fabric was targeted for geochronology.

SY1402 was collected from Lotos (approximate location: 37°26'36.64"N, 24°53'48.87"E). The sample is representative of D_{T2}, during penetrative greenschist-faces deformation and transposition of older fabrics, and some rocks surpass the ductile-to-brittle transition. The sample collected for geochronology is a reaction rind at the margin of a brittlely boudinaged epidote-rich lens, and includes actinolite, chlorite, epidote, phengite, paragonite, and apatite. SY1644 was collected from the southern side of Delfini, very close to KCS1621. The sample is representative of D_{T2}, as rocks locally surpass the ductile-to-brittle transition. Minerals collected for geochronology were precipitated within the boudin neck of a brittlely boudinaged epidote-rich lens including actinolite, epidote, white mica, and calcite.

A2 Compilation of previous geochronology on Syros

Figure A1 and Table A2 show a compilation of published metamorphic geochronology for the island of Syros (through 2019), comprising 185 individual published ages from 16 studies and 5 chronometers. Applying filters discussed in Section 6.2 to the dataset shown in Figure 3B reduces the compilation from 89 (excludes igneous zircon) to 44 data points, which are plotted in Figure 11. The refined dataset comprises 65 individual ages (some presented as weighted means) that include 44 single-grain analyses and 21 isochrons. The single-grain analyses include 6 $^{40}Ar/^{39}Ar$ white mica (Rogowitz et al., 2015; Laurent et

Sample ID and Summary	Phases defining the isochron	Initial Sr	Age	Uncertainty	MSWD	n
SY1616: Kini omphacite-epidote blueschist	paragonite-phengite	0.7032083	53.53	0.17	1	2
	glaucophane-phengite	0.7032228	53.29	0.17	1	2
	omphacite-phengite	0.7032158	53.41	0.17	1	2
	garnet-phengite	0.703212	53.47	0.21	1	2
	epidote-garnet-phengite	0.7032199	53.34	0.15	0.91	3
	epidote-omphacite-phengite	0.7032198	53.34	0.14	0.64	3
	epidote-garnet-omphacite-phengite	0.7032183	53.36	0.14	0.56	4
	glaucophane-omphacite-garnet-phengite	0.7032179	54.37	0.14	0.46	4
	omphacite-paragonite-garnet-phengite	0.7032121	53.47	0.14	0.28	4
	paragonite(x4)-phengite	0.7031964	53.73	0.13	1.4	5
	** ep-glauc-omph-parag-grt ** NO PHENG	0.703221	59.07	8.57	1.7	5
KCS1617: Azolimnos glaucophane-mica blueschist	epidote-phengite	0.7066671	45.14	0.05	1	2
	glaucophane-phengite	0.7065696	45.61	0.1	1	2
	paragonite-phengite	0.7065964	45.48	0.05	1	2
	paragonite-phengite-phengite	0.7065992	45.47	0.05	0.41	3
	glaucophane-phengite-phengite	0.7065829	45.56	0.61	8.8	3
	epidote-phengite-phengite	0.706643	45.23	0.05	31	3
	** glaucophane-paragonite(x4) ** NO PHENG	0.7066026	43.44	0.76	10	5
	paragonite(x4)-phengite	0.7065951	45.48	0.13	9.4	5
	8 point isochron (all data, except garnet)	0.7066036	45.43	0.04	23	8
KCS1621: Delfini actinolite-mica greenschist	** paragonite-chlorite ** NO PHENG	0.7066492	35.64	0.39	1	2
	paragonite-chlorite-phengite	0.7066201	37.04	0.015	13	3
	** epidote-chlorite-paragonite ** NO PHENG	0.7066492	35.64	0.39	7.90E-25	3
	epidote-phengite-phengite	0.7067163	36.9	0.03	6.30E-24	3
	epidote-chlorite-phengite(x2)	0.7066195	37.06	0.02	21	4
	epidote-paragonite-phengite(x2)	0.7066498	37.02	0.02	9.8	4
	** epidote-chlorite-paragonite(x3) ** NO PHENG	0.7066471	36.19	0.29	7.9	5
	paragonite(x3)-phengite(x2)	0.7066348	37.05	0.014	16	5
	chlorite-paragonite(x3)-phengite(x2)	0.7066266	37.06	0.013	16	6
	epidote-chlorite-paragonite(x3)-phengite(x2)	0.7066266	37.06	0.013	13	7
	8 point isochron (all data)	0.7065941	36.91	0.013	440	8
SY1644: Delfini mineralization in epidosite boudin neck	epidote-white mica	0.7066098	36.16	0.03	1	2
	actinolite-white mica	0.7067006	35.94	0.03	1	2
SY1402: Lotos reaction rim around epidosite pod	apatite-phengite1	0.704965	36.49	0.01	1	2
	apatite-phengite2	0.704965	35.94	0.01	1	2
	apatite-phengite3	0.704965	33.18	0.011	1	2
	apatite-phengite4	0.704966	29.43	0.014	1	2

Table A1: Evaluating the robustness of Rb-Sr ages. Various isochrons are calculated for each sample discussed in-text, for different combinations of (assumed) co-genetic phases. MSWD values are a reflection of anaytical uncertainty and the goodness of fit of all data points on a given isochron; therefore, any two-point isochron by definition has an MSWD of 1.

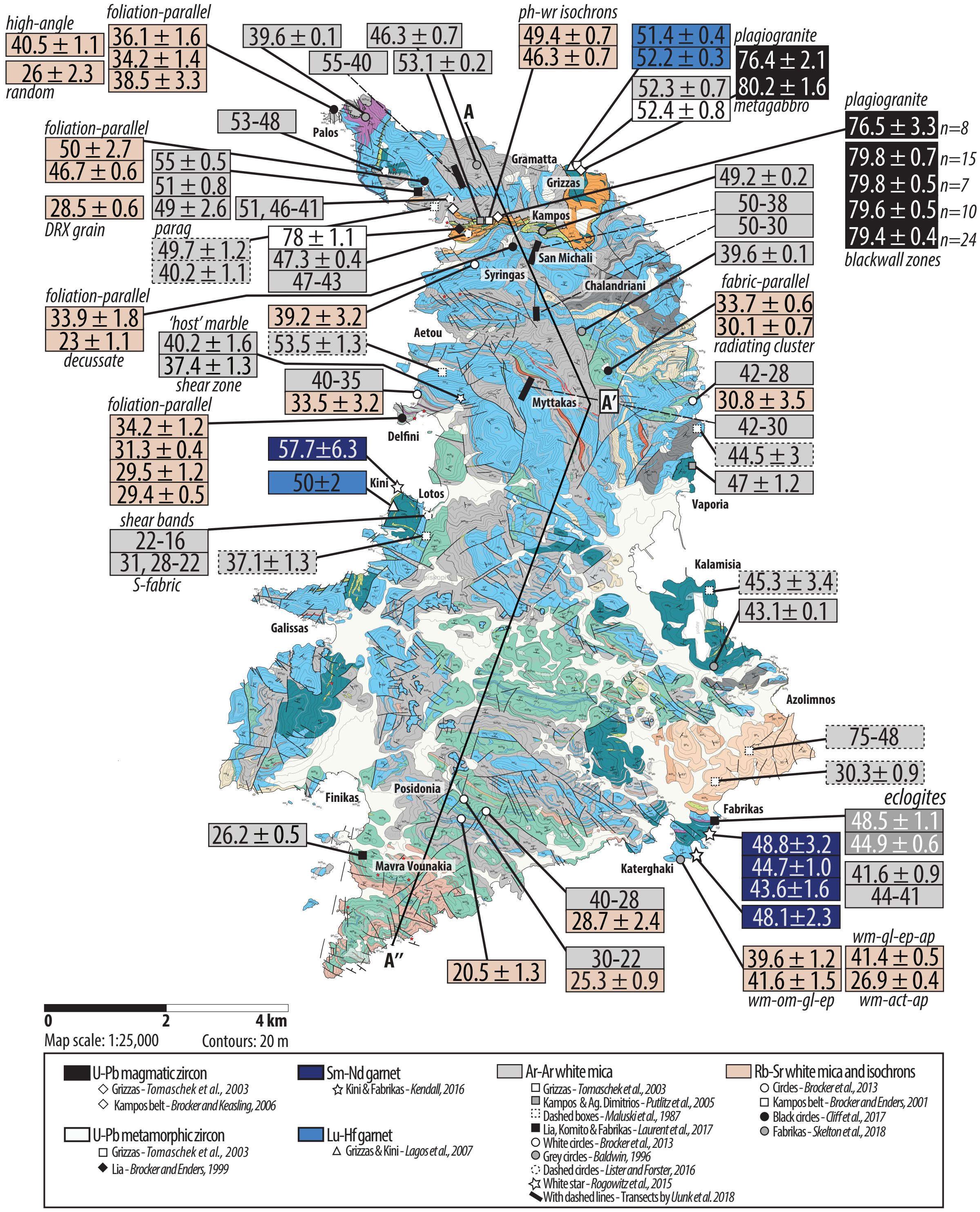

Figure A1: Compilation of the locations and ages from published metamorphic geochronology (and magmatic ages from Kampos), from references listed in grey box and discussed in Section 2. Samples are projected onto the cross-section line A-A'-A" as shown in Figure 11. Sample locations are coded by color and shape according to citation, and box colors around reported ages correspond to different chronometers. Abbreviations for boxes with notes indicating the sample's micro-structural and/or lithologic context are as follows: DRX = dynamically recrystallized; wm=white mica, ph=phengite, om=omphacite, gl=glaucophane, ep=epidote, act=actinolie, ap=apatite, wr=whole rock.

#	Method	Closure Temp	Sample Name and Description	GPS Coordinates^	Location	Age	Uncertainty	Notes	Interpretation*	Ref.
1	**U-Pb zircon**	>750˚C	metagabbro		Grizzas	80.2	1.6		magmatic crystallization (protolith)	[1]
2			meta-plagiogranite dyke		Grizzas	76.4	2.1		magmatic crystallization (protolith)	[1]
3			meta-plagiogranite breccia		Grizzas	52.4	0.8	skeletal rims, low Th/U	HP metamorphism	[1]
4			1081 omphacitite		Kampos belt	78	1		interpreted as HP met, but likely magmatic	[2]
5			4017 plagiogranite in meta-gabbro	37°29.704'N, 024°54.005'E	Kampos belt	77	1	oscillatory zoned zircons	interpreted as HP met, but likely magmatic	[3]
6						76.1	1.2			[3]
7						76.6	1.3			[3]
8						76.6	1.1			[3]
9						76.9	1.1			[3]
10						75	1.2			[3]
11						76.1	1.3			[3]
12						78	1.1			[3]
					average	76.5	3.3			
13			3148 Jadetite: albite + jadeite; accessories	37°29.362'N, 024°54.335'E	Kampos belt blackwall zone	80.3	0.9	oscillatory zoned zircons (likely		[3]
14			titanite, allanite, zircon, white mica, chlorite,			78.7	0.9	magmatic, or seafloor		[3]
15			apatite			80.0	0.9	metasomatism)		[3]
16						78.6	0.7			[3]
17						78.2	0.8			[3]
18						80.6	0.8			[3]
19						78.6	0.7			[3]
20						79.4	0.9			[3]
21						80.7	0.7			[3]
22						79.9	0.7			[3]
23						80.6	0.7			[3]
24						79.8	0.6			[3]
25						77.3	1.4			[3]
26						80.8	0.7			[3]
27						82.9	2.2			[3]
					average	79.8	3.8			
					reported weighted mean	79.8	0.7			
28			3149 Omphacitite: omph, alb, wm, ttn, chl,	37°29.362'N, 024°54.335'E	Kampos belt blackwall zone	79.7	0.5	oscillatory zoned zircons (likely		[3]
29			opaques			79.9	0.3	magmatic, or seafloor		[3]
30						78.5	0.8	metasomatism)		[3]
31						78.4	0.4			[3]
32						76.7	0.5			[3]
33						79.9	1.0			[3]
34						77.6	1.0			[3]
					average	78.7	1.8			
					reported weighted mean	79.8	0.5			
35			3151 Glaucophanite: glaucophane; subordinate	37°29.362'N, 024°54.335'E	Kampos belt blackwall zone	78.9	0.8	oscillatory zoned zircons (likely		[3]
36			amounts of omph, rt, ttn, zrc, all, wm, bt			79.9	0.8	magmatic, or seafloor		[3]
37						78.9	1.2	metasomatism)		[3]
38						79.1	1.2			[3]
39						82.2	1.3			[3]
40						80.0	0.8			[3]
41						78.4	0.7			[3]
42						79.2	0.7			[3]
43						80.3	0.9			[3]
44						80.6	1.0			[3]
					average	79.8	3.0			[3]

Table A2: Compilation of published metamorphic geochronology for Syros Island. Data are plotted against closure temperature in Figure 3B. References: (1) Tomaschek et al. (2003), (2) Bröcker and Enders (1999), (3) Bröcker and Keasling (2006)...

					reported weighted mean	79.6	0.5			
45			3152-A Chlorite Actinolite Zone: chl, act, rt, zrc, wm, ap	37°29.362'N, 024°54.335'E	Kampos belt blackwall zone	77.5	1.8	oscillatory zoned zircons (likely magmatic, or seafloor metasomatism)		[3]
46						80.4	1.3			[3]
47						82.3	2.0			[3]
48						78.5	1.1			[3]
49						80.4	2.1			[3]
50						77.7	1.4			[3]
51						78.2	1.3			[3]
52						79.7	0.7			[3]
53						81.3	1.1			[3]
54						80.0	1.8			[3]
55						78.9	1.1			[3]
56						84.0	3.7			[3]
57						79.9	1.0			[3]
58						81.1	0.8			[3]
					average	80.0	6.2			
59			3152-B Chlorite-Actinolite Zone:	37°29.362'N, 024°54.335'E	Kampos belt blackwall zone	76.2	1.3	oscillatory zoned zircons (likely magmatic, or seafloor metasomatism)		[3]
60						81.3	1.0			[3]
61						79.5	1.0			[3]
62						78.4	1.1			[3]
63						76.9	1.3			[3]
64						73.1	0.7			[3]
65						79.6	0.5			[3]
66						79.3	1.3			[3]
67						78.5	0.8			[3]
68						79.1	0.7			[3]
					average	78.2	3.2			[3]
					reported weighted mean	79.4	0.4			
69	**Sm/Nd garnet**	600-700°C	06MSY-6E rutile-bearing eclogite		Kini	57.7	6.3	8 grt-leachate-wr isochron	garnet growth	[4]
70			14RSY-8A mica-rich eclogite		Fabrikas	48.8	3.2	4 grt-wr isochron	garnet growth	[4]
71			14BSY-35D mica-rich eclogite, float		Fabrikas	48.1	2.3	bulk; grt-grt-grt-wr isochron	garnet growth	[4]
72			14BSY-35D mica-rich eclogite, float		Fabrikas	47.1	3	rim of garnet, microdrilled; rim-rim-rim pwd-matrix isochron	garnet growth	[4]
73			14BSY-38A, eclogite boudin in quartz schist matrix		Fabrikas	44.7	1	5 grt-wr isochron	garnet growth	[4]
74			14BSY-37A eclogite, float		Fabrikas	43.6	1.6	5 grt-wr isochron	garnet growth	[4]
75	**Lu/Hf garnet**	600°C	Ag31: meta-igneous breccia		Grizzas	52.2	0.3	wr-zrn-ttn-'leftover'-4grt isochron; table top digestion	early garnet crystallization (Lu fractionation)	[5]
76			Ag85: meta-igneous breccia		Grizzas	51.4	0.4	wr-omph-'leftover'-4grt isochron; table top digestion	early garnet crystallization (Lu fractionation)	[5]
77			Ap21: glaucophane eclogite		Kini	50	2	wr-omph-'leftover'-3grt isochron; table top digestion	early garnet crystallization (Lu fractionation)	[5]
78	**Rb-Sr WM**	~500°C +/- 50	5243 Ph-Chl-Ab-Qz-Ep-Cal-Ttn-Gr schist	N 37° 23.501' E 24° 54.633'	South Central, Posidonia	28.7	2.4	ph-cal isochron	ages record continuous (partial) resetting of isotopic	[6]
79	**& isochrons**		5244 Ph-Chl-Ab-Qz-Ep-Cal-Ttn schist	N 37° 23.265' E 24° 54.365'	South Central, Posidonia	20.5	1.3	ph-ep-ab isochron	systematics and/or (re)crystallization of white mica	[6]
80			5246 Ph-Pg-Chl-Ab-Qz-Ep-Cal-Ttn schist	N 37° 23.643' E 24° 54.151'	South Central, Posidonia	25.3	0.9	ph-ep-cal isochron	during exhumation and greenschist facies	[6]
81			5267 Ph-Chl-Ab-Qz-Cal-Ttn schist	N 37° 27.734' E 24° 53.898'	N. Delfini	33.5	3.2	ph-cal isochron	retrogression	[6]
82			SYR015 Ph-Pg-Chl-Ab-Qz-Ep-Cal-Ttn schist	N 37° 27.497' E 24° 56.767'	N. of Agios Dimitrios	30.8	2.9	ph-par-ep isochron		[6]

Table A2: Continued. References: (4) Kendall (2016), (5) Lagos et al. (2007), (6) Bröcker et al. (2013)...

83	5831 Ph-Chl-Ab-Qz-Ep-Cal-Ttn-Act schist	N 37° 28.808' E 24° 54.723'	Syringas (S. of Kampos)	39.2	3.2	ph-ep-ab-cal isochron		[6]
84	1081 Omphacitite		Kampos belt	49.4	0.7	ph-wr isochron	interpretation not provided in text; likely crystallizatio	[7]
85	1083 Omphacitite		Kampos belt	46.3	0.7	ph-wr isochron	and/or incipient recrystallization	[7]
86	63286 - calcschist, cal-ph-glc-qz-ab		Palos, Diapori	35.2	1	4 fabric-parallel phengites, 1 randomly oriented aggregate, 2 calcite	Purposefully targeted extensional blueschist- and greenschist-facies fabrics. Phengites were microdrillec from specific microstructures in calc schists and metabasites. Interpreted as "continuous deformation on a regional scale" and exhumation-related (re-)crystallization.	[8]
87				37.4	0.8	*single phengite*		[8]
88				34.4	0.8	*single phengite*		[8]
89				37.5	1.7	*single phengite*		[8]
				36.1	**1.6**	mean of above 4 grains		
90				26	2.3	*randomly oriented phengite*		[8]
91	63297 - calcschist, cal-ph-glc-ep-qz-ab		Palos, Diapori	35.6	0.5	4 fabric-parallel phengites, 1 grain at high angle to fabric, 3 calcite		[8]
92				32.2	0.3	*single phengite*		[8]
93				34.6	1.1	*single phengite*		[8]
94				34.4	0.5	*single phengite*		[8]
				34.2	**1.4**	mean of above 4 grains		
95				40.5	1.1	*high angle phengite, wrapped by foliation-parallel phengites*		[8]
96	63300 - calcschist, cal-ph-glc-chl-qz-ab		Palos, Diapori	41.8	2	4 fabric-parallel phengites, 1 calcite		[8]
97				37.1	0.4	*single phengite*		[8]
98				40.5	0.4	*single phengite*		[8]
99				34.4	0.5	*single phengite*		[8]
				38.5	**3.3**	mean of above 4 grains		
100	63287a - calcschist, cal-ph-grt-dol-glc-qtz-ep-ttn		Grammata	52.5	0.8	6 fabric-parallel phengites, 4 calcite		[8]
101				52.1	1.1	*single phengite*		[8]
102				46.9	2.3	*single phengite*		[8]
103				48.6	0.5	*single phengite*		[8]
				50	**2.7**	mean of above 4 grains		
104	63287b			47.1	0.6	*single phengite*		[8]
105				46.2	1.3	*single phengite*		[8]
				46.7	**0.6**	mean of above 2 grains		
106	63287a			28.5	0.6	*single phengite; has fine grained recrystallized phengite next to it*		[8]
	S97/234 - greenschist, ab-chl-ph-ep-qz-cal, rare glc		N. Oros Syringas			4 fabric-parallel phengites + 3 ep; 1 grain from decussate pressure shadow adjacent to garnet		
107				33.6	0.4	pseudomorph		[8]
108				29.4	2.3	*single phengite*		[8]
109				34	0.5	*single phengite*		[8]
				33.9	**1.8**	weghted mean of above 3 grains		
110				23	1.1	*decussate phengite*		[8]
111	63301 - greenschist, qz-ph-chl-ab-cal-dol-ttn-ap pg		Foinikia	30.1	0.7	*decussate/radiating cluster at high angle to fabric*; plus 2 cal + 2 ttn		[8]
112				33.7	0.6	*composite fabric-parallel sample*		[8]
113	63310 - blueschist, ep-glc-ph-cal-qz-ab-ttn-tour chl		Delfini	31.3	0.4	2 phengite composite samples aligned with schistosity; 3 ep + 2 cal		[8]

Table A2: Continued. References: (7) Bröcker and Enders (2001), (8) Cliff et al. (2016)...

114						29.5	1.2	*composite #2*		[8]
115			63314 - blueschist, ph-glc-qz-ep-ttn-chl-ab-cal-ap		Delfini	34	1.7	8 fabric-parallel phengites, 1 epidote, 1 apatite, 2 ttn, lots of ep inclusions		[8]
116						39.5	3.1	*single phengite*		[8]
117						33.9	1.2	*single phengite*		[8]
118						36.3	1.3	*single phengite*		[8]
119						34.3	1.2	*single phengite*		[8]
120						33.7	0.6	*single phengite*		[8]
						34.2	**1.3**	regression of above six grains w. epidote		
121						29.7	0.7	*single phengite*		[8]
122						29.2	0.7	*single phengite*		[8]
						29.4	**0.5**	weighted mean of youngest grains		
				GPS points approximated from map, not provided in text						
123			15-SY-03 glaucophane eclogite	37°23'20.99"N 24°57'13.35'	Fabrikas	39.6	1.2	4wm-omph-glauc-ep isochron	Interpreted as peak metamorphism, but probably	[9]
124			15-SY-05 glaucophane eclogite		Fabrikas	41.6	1.5	4wm-omph-glauc-ep-ap isochron	'reworked' during exhumation	[9]
125			15-SY-01-02 epidote blueschist	37°23'17.66"N 24°57'9.50"I	Fabrikas	41.36	0.45	4wm-glauc-ep-ap isochron		[9]
126			17 FB 05 greenschist		Fabrikas	26.9	0.4	wm-act-ap isochron	greenschist recrystallization	[9]
127	**Ar/Ar WM**	~400-450˚C	AG144 and BSY260 meta-plagiogranite dyke & breccia		Grizzas	52.3	0.7	Ar steps yield apparent ages between 30-54 Ma	prograde crystallization?	[1]
128		550˚C (Ref. 11)								
129			SY01 metachert		North of Delfini	53.5	1.3		prograde?	[10]
130			SY15 metatuff		North of Ag. Dimitrios	44.5	3		(partial) resetting and/or recrystallization	[10]
131			SY30F eclogitic metagabbro		W. Kampos belt	40.2	1.1		(partial) resetting and/or recrystallization	[10]
132			SY501 omphacitic metagabbro		North of Fabrikas	30.3	0.9		(partial) resetting and/or recrystallization	[10]
133			SY7 calcschist-metatuff		East of Kini	37.1	1.3		(partial) resetting and/or recrystallization	[10]
134			SY66 omphacitic metagabbro		Airport	45.3	3.4		(partial) resetting and/or recrystallization	[10]
135			SY08 calcschist		W. Kampos belt	49.7	1.2	paragonite	Prograde? Or partial resetting?	[10]
136			SY20 metagranite		Vari	48 to 75		no Eocene HP history in Vari Unit	Metamorphic crystallization	[10]
137			S07-14 Grt-Omph blueschist	37.4992/24.8935	Grammata	50.84	0.84	single grain (2)	peak conditions	[11]
138						49.44	2.62		peak conditions	[11]
139			S07-16 Grt-Chl micaschist	37.4992/24.8935	Grammata	55.04	0.56	concentrate	peak conditions	[11]
140			S07-01 Gln-Ep micaschist	37.3891/24.9534	Fabrikas	41.65	0.95	single grain	recrystallization	[11]
141			S07-02 Blueschist	37.3891/24.9534	Fabrikas	43.51	0.56	single grain (2)	recrystallization	[11]
142						41.95	0.77		recrystallization	[11]
143			S07-04 Gln eclogite	37.3891/24.9534	Fabrikas	44.89	0.65	single grain	peak in intermediate unit?	[11]
144			S07-04bis Gln eclogite	37.3891/24.9534	Fabrikas	40.29	0.73	single grain	recrystallization	[11]
145			S07-jojo Gln eclogite	37.3891/24.9534	Fabrikas	48.5	1.1	in situ (10), isochron reported	peak in intermediate unit?	[11]
146			S07-17 Alb-Chl micaschist	37.3791/24.8819	NW of Komito Beach	26.12	0.52	single grain	recrystallization	[11]
147			5267 Ph-Chl-Ab-Qz-Cal-Ttn schist	N 37˚ 27.734' E 24˚ 53.898'	N. Delfini	35-40		10 grains	Ar ages span 41-27; Rb-Sr ages span 34-20	[6]
148			SYR015 Ph-Pg-Chl-Ab-Qz-Ep-Cal-Ttn schist	N 37˚ 27.497' E 24˚ 56.767'	N. of Agios Dimitrios	28-42		12 grains, excludes 1 outlier	Ages record continuous (partial) resetting of isotopic	[6]
149			5243 Ph-Chl-Ab-Qz-Ep-Cal-Ttn-Gr schist	N 37˚ 23.501' E 24˚ 54.633'	South Central, Posidonia	28-40		12 grains	systematics and/or (re)crystallization of white mica	[6]
150			5246 Ph-Pg-Chl-Ab-Qz-Ep-Cal-Ttn schist	N 37˚ 23.643' E 24˚ 54.151'	South Central, Posidonia	22-30		13 grains	during exhumation and greenschist facies	[6]
151			89646 quartzite		Palos	39.6	0.1	total fusion age, gradient in apparent ages 31 to 41.2	partial loss profile and/or recrystallization after HP ev	[12]
152			89644 glaucophane-marble schist		Kampos belt	53.1	0.2	phengite, total fusion age, graident 52.4 to 55	HP event	[12]
153			89642 retrograde eclogite		Kampos belt	49.2	0.2	phengite, flat spectra, weighted mean	HP event	[12]

Table A2: Continued. References: (9) Skelton et al. (2019), (10) Maluski et al. (1987), (11) Laurent et al. (2017), (12) Baldwin (1996)...

154	89645 retrograde blueschist		Central	39.6	0.1	total fusion age, gradient 34.8 to 42.4	partial loss profile and/or recrystallization after HP event	[12]
155	89649 retrograde blueschist		Airport	43.05	0.12	total fusion age, gradient 40 to 44.2	partial loss profile and/or recrystallization after HP event	[12]
156	SY-7 phengite-rich eclogite		Kampos belt	46.3	0.7	in-situ UV-laser ablation; weighted mean laser fusion ages (n=27)	paper says prograde; could be partially reset, some ages are older (50-52)	[13]
157	SY-25 omphacite-rich meta-gabbro		Agios Dimitrios	47	1.2	in-situ UV-laser ablation; weighted mean laser fusion ages (n=30)	paper says prograde; our observations of Ag. Dim indicate this is likely recrystallization and/or neo-crystallization	[13]
							All ages from [14] are interpreted as crystallization ages related to different microstructures using the 'method of asymptotes and limits'	
158	AG10-31 garnet mica schist	37° 30.081'N 24° 53.173'E	N. of Gramatta	53-48		ΔIB + early ΔIC decussate + post-ΔIC shear zone, pheng-muscovite	timing of ΔIB event	[14]
159	AG10-14 garnet mica schist	37° 29.613'N 24° 54.295'E	N. Kampos belt	51, 46-41		ΔIB + ΔIC + post-ΔIC, older phengite component, younger muscovite component	muscovite component records ΔIC growth and post-ΔIC shearing	[14]
160	AG10-15 ΔIC white mica in boudin neck	37° 29.537'N 24° 54.416'E	Kampos belt	43-47		late ΔIC porphyroblastic white mica from dilational zone next to mega-boudin		[14]
161	AG10-16 early ΔIC decussate wm + titanite	37° 29.546'N 24° 54.404'E	Kampos belt	47.3	0.4	early ΔIC decussate white mica, from edge of mega-boudin		[14]
162	AG10-26S wm-qz-ab-chl-calc greenschist	37° 26.582'N 24° 54.166'E	E. of Kini, roads above Lotos	31, 28-22		Dominant fabric in greenschist facies schist (post-ΔID and Δ2)	older phengite component; younger muscovite component	[14]
163	AG10-26C wm-qz-ab-chl-calc greenschist	37° 26.582'N 24° 54.166'E	E. of Kini, roads above Lotos	16-22		Extensional shear bands cutting greenschist fabric (relict post-ΔID + Δ2 + post-Δ2)	muscovite component	[14]
	Kampos transect - *graphite-rich Lws-Grt blueschists and micaschists, with intercalated calcite and siliceous layers*		N. of Kampos belt			*single grain fusion experiments*		
164	12SR100: graphite-rich Lws-Grt-Gln micaschist, static gscht.	N37° 29.855', E24° 54.369'		55-48		broad uniform age		[15]
165	12SR57: siliceous marble; Phg+Gln+ Ep+Qz+ Ttn+Chl	N37° 29.856', E24° 54.220'		55-48		broad uniform age		[15]
166	12SR02: graphite-rich Lws(ps)-Grt-Gln micaschist; ttn in foliation	N37° 29.942', E24° 54.566'		52-45		wide uniform age		[15]
167	12SR97: Phg+Qz+Ep+Ttn bearing marble	N37° 29.827', E24° 54.628'		52-45		wide uniform age		[15]
168	12SR03: phg-bearing marble with columnar aragonite pseudomorphs	N37° 29.821', E24° 54.744'		55-40		heterogeneous		[15]
	San Michalis transect - *marble-schist-marble sequence, middle unit contains pyrite-bearing schists and gneisses, graphite-rich Lws-Grt-Gln micaschists and quartzitic rocks, locally with static greenschist overprint*		S. of Kampos belt			*single grain fusion experiments*		
169	12SR96: Lws-Grt-Gln micaschist, static gscht	N37°29.393', E24°54.891'		49-45		narrow range		[15]
170	12SR04: Lws-Grt-Gln micaschist, static gscht	N37°29.359', E24°55.125'		48-40		heterogeneous		[15]
171	12SR13b: carbonated and brecciated blueschist; Ctd-Gln, Ep	N37°29.328', E24°55.223'		48-40		heterogeneous		[15]

Table A2: Continued. References: (13) Putlitz et al. (2005), (14) Lister and Forster (2016), (15) Uunk et al. (2018).

172	12SR92: Phg-bearing marble; aragonite pseudomorphs	N37°29.395', E24°54.975'		48-40		heterogeneous		[15]
173	12SR93: Phg-bearing marble; aragonite pseudomorphs	N37°29.343', E24°54.904'		50-38		heterogeneous		[15]
	Syringas transect 1 and 2 *- intercalated schist-marble sequence; vary from felsic to Ep-blueschists to pervasively overprinted greenschists*		Sy1 west coast; Sy2 central			*single grain fusion experiments*		
174	12SR78: crenulated felsic mica schist	N37°28.830', E24°53.901'		48-42		narrow uniform age		[15]
175	12SR82: calcschist, Phg+Qz+Chl	N37° 28.666', E24° 55.119'		38-31		intermediate		[15]
176	12SR81: Phg-bearing marble, aragonite pseudon	N37° 28.664', E24° 55.118'		50-40		heterogeneous		[15]
	Myttakas transect *- upper and lower marbles bookending felsic schists and gneisses and intermediate-mafic rocks ranging from ep-grt blueschists to pervasively overprinted greenschists*		NE of Delfini, central			*single grain fusion experiments*		
177	12SR19: Phg-bearing marble	N37°27.889', E24°55.225'		40-39		narrow uniform age		[15]
178	12SR16: Ep-Ab blueschist (+Grt), partial greenschist overprint	N37°27.796', E24°55.147'		40-39		narrow uniform age		[15]
179	12SR20: felsic Ab gneiss; Phg+Qz foliation, Ab porphyroblasts	N37°27.871', E24°55.199'		42-30		heterogeneous		[15]
180	12SR18b: intermediate-to-mafic Grt-Ep blueschist; Phg+Gln+Ep matrix	N37°27.841', E24°55.174'		42-30		heterogeneous		[15]
181	12SR18a: blueschist, static greenschist; Phg+Qz matrix	N37°27.811', E24°55.171'		42-30		heterogeneous		[15]
182	12SR17: greenschist mylonite, fine-grained Act+Chl matrix, Ab blasts	N37°27.798', E24°55.154'		42-30		heterogeneous		[15]
183	12SR15: siliceous marble, Ep+Phg+Qz, aragonite pseudomorphs	N37°27.808', E24°55.101'		42-30		heterogeneous		[15]
184	Calcite marble intercalated with quartz and dolon ?		N. of Delfini	40.2	1.6	Si apfu 3.4-3.6	Authors hypothesized these would be Miocene due to strong EW stretching. Interpreted Eocene ages as evidence that the phengite was not reset during Miocene deformation; our results suggest these could be DT2 greenschist deformation	[16]
185	Shear zone			37.4	1.3			

Table A2: Continued. References: (16) Rogowitz et al. (2015).

al., 2017), 37 ^{87}Rb/^{86}Sr white mica (Cliff et al., 2016), and 1 U-Pb SHRIMP zircon age which is a weighted mean of 7 analyses (Tomaschek et al., 2003). The isochrons include 5 Sm-Nd garnet-whole rock (Kendall, 2016), 3 Lu-Hf garnet-omphacite-whole rock (Lagos et al., 2007), 10 multi-mineral and 2 phengite-whole rock ^{87}Rb/^{86}Sr (Bröcker & Enders, 2001; Bröcker et al., 2013; Skelton et al., 2019), and one 10-point inverse ^{40}Ar/^{39}Ar (Laurent et al., 2017)). The ^{40}Ar/^{39}Ar ages included in the final compilation are in-situ analyses of grains in thin section (used to construct the 10-point inverse isochron), and strong plateaus from step-heating experiments of grains extracted from well-characterized microstructural domains (Laurent et al., 2017). We excluded: 1 Sm-Nd isochron with low ^{147}Sm/^{144}Nd ratio and potential for contamination due to the presence of an off-isochron inclusion (cf. Kendall, 2016); and 50 ^{40}Ar/^{39}Ar ages that exhibit one or more of the complications described above (Maluski et al., 1987; Baldwin, 1996; Tomaschek et al., 2003; Putlitz et al., 2005; Bröcker et al., 2013; Lister & Forster, 2016; Laurent et al., 2017; Uunk et al., 2018).

Lagos et al. (2007) presented Lu-Hf garnet growth ages from meta-igneous rocks at Grizzas and Kini, showing that those blueschist-eclogite localities reached peak metamorphic conditions at 51.9±1.4 Ma and 50±2 Ma, respectively. New fabric ages from Kini blueschists (this study, 52.62 ± 0.64 Ma) overlap with garnet growth ages at Grizzas and Kini, and with the SHRIMP age determined by Tomaschek et al. (2003) for Grizzas metamorphic zircons.

Fabrikas eclogites record Sm-Nd garnet crystallization ages of ∼45±3 Ma (Kendall, 2016). 'Bulk' garnet ages (48.1±2.3 Ma) overlap within error with 'rim' ages (47.1±3 Ma), providing evidence for rapid, pulsed garnet crystallization that is distinctly younger than Grizzas and Kini. Garnet growth ages are consistent with ^{40}Ar/^{39}Ar ages of foliation-forming white mica in Fabrikas glaucophane-bearing eclogites (48.5±1.1 Ma to 44.9±0.6 Ma, Laurent et al. (2017)).

Retrograde blueschist-facies fabric ages range from ∼50-40 Ma, and are captured by: (1) Phengite-whole rock Rb-Sr isochrons from omphacitites at Kampos (49.4±0.7 Ma and 46.3±0.7 Ma, Bröcker and Enders (2001)) and Rb-Sr ages of micro-drilled phengites from glaucophane-bearing calcschists at Gramatta (50.5±3.1 Ma and 47.3±1.2 Ma, Cliff et al. (2016)); (2) A new multi-mineral Rb-Sr isochron from Azolimnos (44.71 ± 0.43 Ma, this study); (3) A Rb-Sr isochron from omphacite-blueschists (41.5±1.5 Ma, Skelton et al. (2019)) and ^{40}Ar/^{39}Ar ages of foliation-forming white mica in retrogressed Fabrikas eclogites and bluechists (44.9±0.65 Ma to 40.3±0.7 Ma, n=4, Laurent et al. (2017)).

Retrograde greenschist-facies fabric ages range from ∼42-36 Ma, and are captured by Rb-Sr multi-mineral isochrons and Rb-Sr ages of foliation-forming micro-drilled phengites from greenschists and calcschists from the following locations: (1) Palos (40.5±1.1 Ma to 34.2±1.4 Ma, Cliff et al. (2016)); (2) Syringas (39.2±3.2 Ma, Bröcker et al. (2013); 33.9±1.8 Ma Cliff et al. (2016)); (3) North of Delfini (33.7±0.6 Ma, Cliff et al. (2016); 33.5±3.2 Ma and 30.8±2.9 Ma, Bröcker et al. (2013)); (4) Delfini (34.2±1.3 Ma to 29.4±0.5 Ma; Cliff et al. (2016); 36.47±0.11 Ma, this study); (5) Fabrikas (26.9±0.4 Ma, Skelton et al. (2019)); and (6) Posidonia (28.7±2.4 Ma, 25.4±0.9 Ma, 20.5±1.3 Ma, Bröcker et al. (2013)).

Appendix B Electron Microprobe Techniques and Data Treatment

B1 Qualitative X-Ray Mapping

Qualitative X-Ray compositional maps were acquired on the JEOL JXA-8200 electron microprobe at the University of Texas at Austin. Polished 30 μm thin sections were analyzed using a 15 kV accelerating voltage, focused beam, 300 nA current, 6 μm step size, and 1 ms dwell time. X-ray maps for Si, Al, Ca, Mg, Fe, Na, K, Mn, Ti, and P were collected. Post-processing to produce false color compositional maps creation was done in ImageJ software by merging element channels with assigned colors.

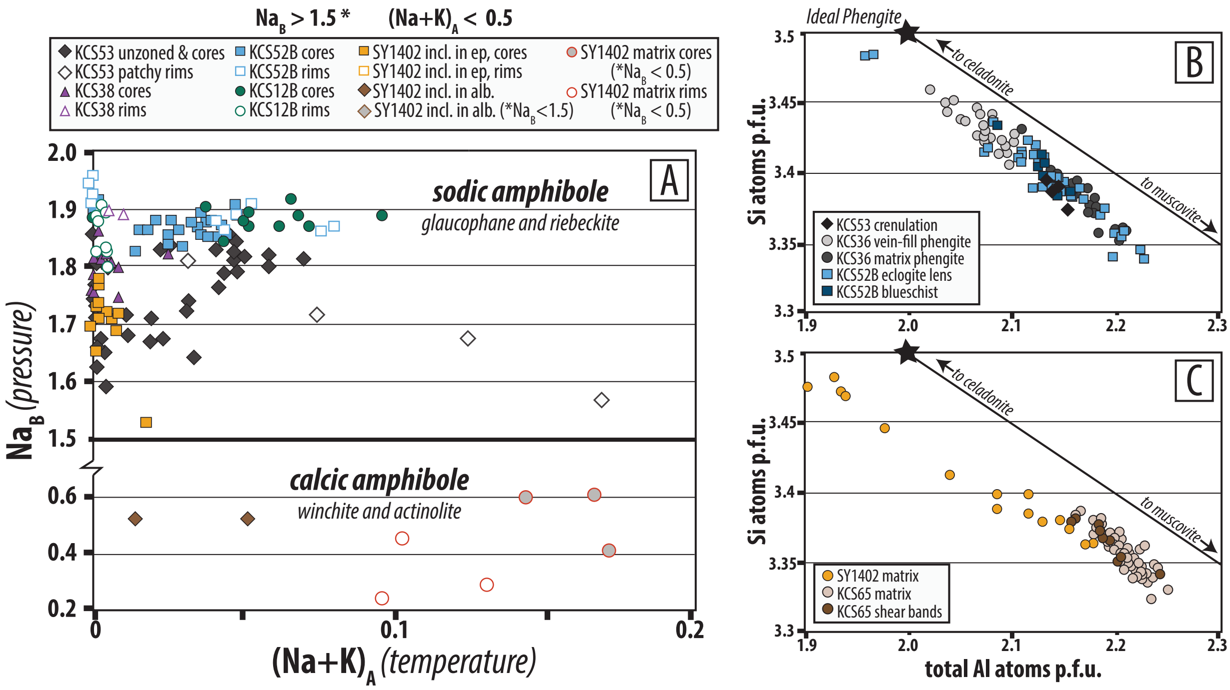

Figure B1: Quantitative EPMA results for (A) amphiboles and (B,C) white micas. (A) Na_B and $(Na+K)_A$ in amphibole are qualitative indicators of pressure and temperature, respectively. Temperature is less reliable since all of these amphiboles are very 'cold' (i.e. crystallize at <500°). Sodic amphiboles correspond to D_S and D_{T1}, and calcic amphiboles correspond to D_{T2}; see text for significance of core-rim zonations and compositional trends during deformation. (B) D_S and D_{T1} white mica chemistry. Elevated Si apfu indicates HP metamorphism. (C) D_{T2} white mica chemistry. Grains cluster towards a lower Si apfu on average, which reflects more pervasive recrystallization under lower P conditions. Intergrown phengite and paragonite is common during all deformation stages. CBU samples do not contain the limiting assemblage required for Si-in-phengite geobarometry calibrated by (Massonne & Schreyer, 1987). However, they do contain other stable Fe-Mg buffering phases (e.g. epidote, amphibole), so within a given sample and between samples of similar bulk compositions, Si variability is a reasonable measure of *relative* changes in pressure, not absolute. Samples in (B) are all meta-mafics, SY1402 in (C) is meta-mafic, KCS65 in (C) is a quartz-rich mixed meta-volcanic/meta-sediment.

B2 Quantitative Point Analyses

Quantitative analyses were collected for representative amphiboles and micas on the JEOL JXA-8200 electron microprobe at the University of Texas at Austin. Samples were selected to cover the range of interpreted structural contexts determined during field work and microstructural analysis. Polished 30 μm thin sections were analyzed using a 15 kV accelerating voltage, a 1μm beam diameter amphibole and a 10μm beam diameter for mica, 10 nA current, and counting time 30 s for all elements. Synthetic compounds and homogeneous minerals were used as standards, and secondary standards were analyzed throughout analytical procedures. Data were processed using the JEOL ZAF procedure.

Sample:	**KCS53**	***n=30***	**KCS53**	***n=6***	**KCS53**	***n=4***	**KCS53**	***n=10***	**KCS38**	***n=14***	**KCS38**	***n=2***	**KCS52B**	***n=21***	**KCS52B**	***n=4***	**KCS52B**	***n=8***	**KCS52B**	***n=3***
Context:	*matrix cores*		*cren. limb cores*		*cren. limb rims*		*cren. hinges*		*matrix cores*		*matrix rims*		*ecl, cores*		*ecl, rims*		*matrix cores*		*matrix rims*	
SiO2	58.71	0.54	58.67	0.32	57.09	1.04	58.60	0.18	59.25	0.22	58.87	0.30	58.54	0.49	58.07	0.20	58.53	0.33	58.03	0.42
Al2O3	11.23	0.20	11.07	0.05	11.00	0.12	11.07	0.15	11.78	0.26	11.59	0.13	10.83	0.72	10.11	0.10	11.26	0.20	10.72	0.43
K2O	0.01	0.01	0.01	0.01	0.03	0.02	0.01	0.01	0.01	0.01	0.00	0.00	0.00	0.01	0.00	0.00	0.01	0.00	0.00	0.00
Na2O	6.54	0.24	7.06	0.11	6.80	0.29	7.13	0.11	6.93	0.16	7.21	0.04	7.20	0.10	7.13	0.01	7.26	0.09	7.22	0.09
CaO	0.97	0.38	0.80	0.14	1.54	0.87	0.70	0.23	0.91	0.16	0.20	0.01	0.32	0.18	0.13	0.04	0.34	0.12	0.12	0.08
MnO	0.06	0.04	0.04	0.01	0.10	0.05	0.05	0.02	0.03	0.02	0.09	0.01	0.11	0.08	0.19	0.02	0.06	0.03	0.17	0.06
FeO	9.16	0.55	9.02	0.18	10.19	0.53	9.33	0.43	7.71	0.50	11.05	0.53	11.09	2.27	14.25	0.23	9.39	0.79	11.95	0.66
MgO	11.43	0.37	11.64	0.21	11.30	0.62	11.52	0.41	11.65	0.51	9.67	0.28	10.28	1.16	8.68	0.04	11.04	0.50	9.59	0.48
TiO2	0.03	0.03	0.00	0.01	0.02	0.03	0.02	0.03	0.02	0.02	0.03	0.01	0.01	0.02	0.02	0.02	0.01	0.02	0.01	0.02
Cr2O3	0.02	0.02	0.02	0.02	0.00	0.00	0.02	0.02	0.01	0.02	0.00	0.00	0.01	0.02	0.03	0.01	0.02	0.02	0.00	0.01
Total	97.89	0.47	98.30	0.26	98.05	0.13	98.44	0.25	98.29	0.49	98.68	0.26	98.37	0.27	98.58	0.15	97.88	0.31	97.79	0.71
Si	7.96	0.05	7.94	0.03	7.81	0.12	7.92	0.03	7.97	0.05	8.00	0.00	7.97	0.02	7.99	0.02	7.96	0.02	7.97	0.02
Al (iv)	0.04	0.04	0.06	0.03	0.19	0.12	0.08	0.03	0.04	0.04	0.00	0.00	0.03	0.02	0.01	0.02	0.04	0.02	0.03	0.02
K (A)	0.00	0.00	0.00	0.00	0.00	0.00	0.00	0.00	0.00	0.00	0.00	0.00	0.00	0.00	0.00	0.00	0.00	0.00	0.00	0.00
Na (A)	0.01	0.01	0.04	0.01	0.10	0.05	0.05	0.01	0.01	0.01	0.01	0.00	0.02	0.02	0.00	0.00	0.04	0.01	0.01	0.02
Na (B)	1.71	0.06	1.81	0.02	1.70	0.12	1.82	0.03	1.80	0.04	1.89	0.00	1.88	0.04	1.90	0.00	1.88	0.02	1.91	0.04
Ca (B)	0.14	0.06	0.12	0.02	0.23	0.13	0.10	0.03	0.13	0.02	0.03	0.00	0.05	0.03	0.02	0.01	0.05	0.02	0.02	0.01
Mn (B, 2+)	0.01	0.00	0.00	0.00	0.01	0.01	0.01	0.00	0.00	0.00	0.01	0.00	0.01	0.01	0.02	0.00	0.01	0.00	0.02	0.01
Fe (B, 2+)	0.11	0.04	0.07	0.01	0.06	0.01	0.07	0.02	0.04	0.04	0.07	0.00	0.06	0.03	0.05	0.01	0.07	0.02	0.05	0.04
Fe (C, 2+)	0.91	0.06	0.82	0.05	0.91	0.09	0.83	0.08	0.81	0.09	1.16	0.05	1.02	0.19	1.32	0.04	0.89	0.09	1.11	0.05
Fe (C, 3+)	0.02	0.03	0.13	0.04	0.20	0.05	0.16	0.04	0.01	0.02	0.03	0.01	0.19	0.13	0.27	0.05	0.11	0.03	0.21	0.10
Al (C, vi)	1.75	0.05	1.70	0.03	1.58	0.10	1.69	0.04	1.83	0.02	1.85	0.01	1.71	0.09	1.63	0.03	1.76	0.03	1.71	0.04
Mg (C)	2.31	0.07	2.35	0.05	2.31	0.13	2.32	0.08	2.34	0.09	1.96	0.05	2.08	0.22	1.78	0.01	2.24	0.09	1.97	0.08
Type	***Glaucophane***		***Glaucophane***		***Glaucophane***		***Glaucophane***		***Glaucophane***		***Glaucophane***		***Glaucophane***		***Mg-Riebeckite***		***Glaucophane***		***Glaucophane***	

Table B1: Amphibole mineral chemistry. Reported values are averages of the number of spots indicated by n values for each sample and micro-textural context. Uncertainties reflect the range of measured values for each micro-textural context as indicated. Cations per formula unit are calculated for ideal element partitioning for 23 Oxygen atoms.

Sample:	**KCS52B** *n=6*		**KCS52B** *n=7*		**KCS12B** *n=11*		**KCS12B** *n=8*		**SY1402** *n=8*		**SY1402** *n=10*		**SY1402** *n=1*		**SY1402** *n=2*		**SY1402** *n=3*		**SY1402** *n=2*	
Context:	*ps, cores*		*ps, rims*		*matrix cores*		*matrix rims*		*incl. in ep, cores*		*incl. in ep, rims*		*incl. in alb (A)*		*incl. in alb (B)*		*matrix cores*		*matrix rims*	
SiO2	58.58	0.20	57.72	0.42	56.32	0.22	54.03	0.63	57.78	0.15	57.30	0.69	58.28		56.52	1.24	54.13	0.26	54.93	0.96
Al2O3	11.35	0.13	10.65	0.44	10.72	0.38	4.92	1.61	8.12	0.87	8.45	1.28	8.05		2.80	0.89	3.12	0.16	2.23	0.60
K2O	0.00	0.01	0.00	0.00	0.00	0.00	0.02	0.01	0.02	0.01	0.03	0.03	0.05		0.19	0.14	0.12	0.03	0.09	0.03
Na2O	7.18	0.06	7.24	0.08	7.09	0.14	6.65	0.22	6.50	0.21	6.39	0.33	6.45		1.89	0.06	2.49	0.40	1.32	0.17
CaO	0.48	0.06	0.24	0.13	0.29	0.11	0.66	0.33	0.73	0.33	0.93	0.88	1.14		8.92	0.23	8.58	0.99	10.80	0.26
MnO	0.05	0.01	0.14	0.06	0.06	0.03	0.14	0.03	0.15	0.07	0.16	0.07	0.21		0.32	0.01	0.40	0.05	0.38	0.03
FeO	9.08	0.27	12.51	1.43	16.93	0.49	25.10	2.03	15.28	1.08	15.55	1.60	14.41		12.24	1.06	15.64	1.74	12.16	0.79
MgO	11.23	0.34	9.45	0.66	6.50	0.20	5.85	0.25	9.74	0.48	9.29	0.87	10.32		14.93	1.43	13.92	1.11	16.77	0.74
TiO2	0.01	0.02	0.01	0.03	0.02	0.03	0.02	0.02	0.02	0.03	0.03	0.03	0.00		0.00	0.00	0.02	0.01	0.01	0.01
Cr2O3	0.00	0.00	0.01	0.02	0.01	0.01	0.00	0.00	0.00	0.00	0.00	0.00	0.00		0.00	0.00	0.00	0.00	0.00	0.00
Total	97.92	0.45	97.93	0.33	97.92	0.29	97.35	0.36	98.33	0.41	98.11	0.62	98.91		97.80	0.85	98.42	0.20	98.69	0.42
Si	7.95	0.02	7.95	0.02	7.93	0.04	7.85	0.04	8.01	0.04	7.98	0.07	8.01		8.01	0.05	7.73	0.06	7.74	0.08
Al (iv)	0.05	0.02	0.05	0.02	0.07	0.04	0.15	0.04	0.01	0.02	0.03	0.05	0.00		0.02	0.02	0.27	0.06	0.26	0.08
K (A)	0.00	0.00	0.00	0.00	0.00	0.00	0.00	0.00	0.00	0.00	0.01	0.00	0.01		0.03	0.03	0.02	0.00	0.02	0.00
Na (A)	0.03	0.01	0.04	0.03	0.05	0.02	0.00	0.00	0.00	0.00	0.00	0.00	0.00		0.00	0.00	0.14	0.02	0.10	0.02
Na (B)	1.86	0.01	1.89	0.03	1.88	0.02	1.87	0.05	1.75	0.05	1.73	0.09	1.72		0.52	0.01	0.55	0.12	0.26	0.03
Ca (B)	0.07	0.01	0.04	0.02	0.04	0.02	0.10	0.05	0.11	0.05	0.14	0.13	0.17		1.35	0.01	1.31	0.15	1.63	0.03
Mn (B, 2+)	0.01	0.00	0.02	0.01	0.01	0.00	0.02	0.00	0.02	0.01	0.02	0.01	0.02		0.04	0.00	0.05	0.01	0.05	0.00
Fe (B, 2+)	0.07	0.02	0.06	0.02	0.07	0.02	0.01	0.01	0.11	0.02	0.10	0.04	0.08		0.05	0.03	0.09	0.03	0.06	0.00
Fe (C, 2+)	0.86	0.06	1.16	0.15	1.74	0.06	1.71	0.06	1.28	0.12	1.35	0.15	1.20		1.36	0.16	1.38	0.16	1.07	0.05
Fe (C, 3+)	0.10	0.03	0.22	0.08	0.18	0.03	1.33	0.28	0.39	0.16	0.36	0.18	0.38		0.03	0.05	0.40	0.05	0.30	0.06
Al (C, vi)	1.77	0.02	1.68	0.06	1.71	0.04	0.69	0.29	1.32	0.13	1.36	0.17	1.31		0.45	0.13	0.26	0.05	0.11	0.03
Mg (C)	2.27	0.06	1.94	0.12	1.36	0.04	1.27	0.05	2.01	0.10	1.93	0.17	2.12		3.15	0.25	2.96	0.23	3.52	0.13
Type	***Glaucophane***		***Glaucophane***		***Riebeckite***		***Riebeckite***		***Mg-Riebeckite***		***Mg-Riebeckite***		***Mg-Riebeckite***		***Winchite***		***Fe-Winchite***		***Actinolite***	

Table B1: Continued. Amphibole mineral chemistry. Reported values are averages of the number of spots indicated by n values for each sample and micro-textural context. Uncertainties reflect the range of measured values for each micro-textural context as indicated. Cations per formula unit are calculated for ideal element partitioning for 23 Oxygen atoms.

B3 Mineral classification and formula unit calculations

Quantitative point analyses for amphiboles and white micas were converted from oxide percentage to atoms per formula unit on the basis of 22O + 2OH, and 10O + 2OH Oxygen atoms, respectively. Amphibole sub-groups and species were determined following recommendations of the Commission on New Minerals Nomenclature and Classification (CNMNC) of the International Mineralogical Association (IMA) (Hawthorne et al., 2012), and species names follow the (Leake et al., 1997) classification scheme. Classifications did not assume initial M-site$^{3+}/\sigma$M-site ratios, so ferric iron components were estimated based on charge balance by adjusting valences of Fe and Mn by automatically normalizing the cations. Data shown here commonly fell into the "sum Si to Ca=15", "sum Si to Mg=13", and "sum Si to Na=15" normalization schemes (Hawthorne et al., 2012). Hydroxyl contents were not estimated using OH=2-2Ti, and initial H_2O contents were not required for calculations. White mica ferric iron was ignored in formula calculations.

Appendix C Supplemental Field Photos

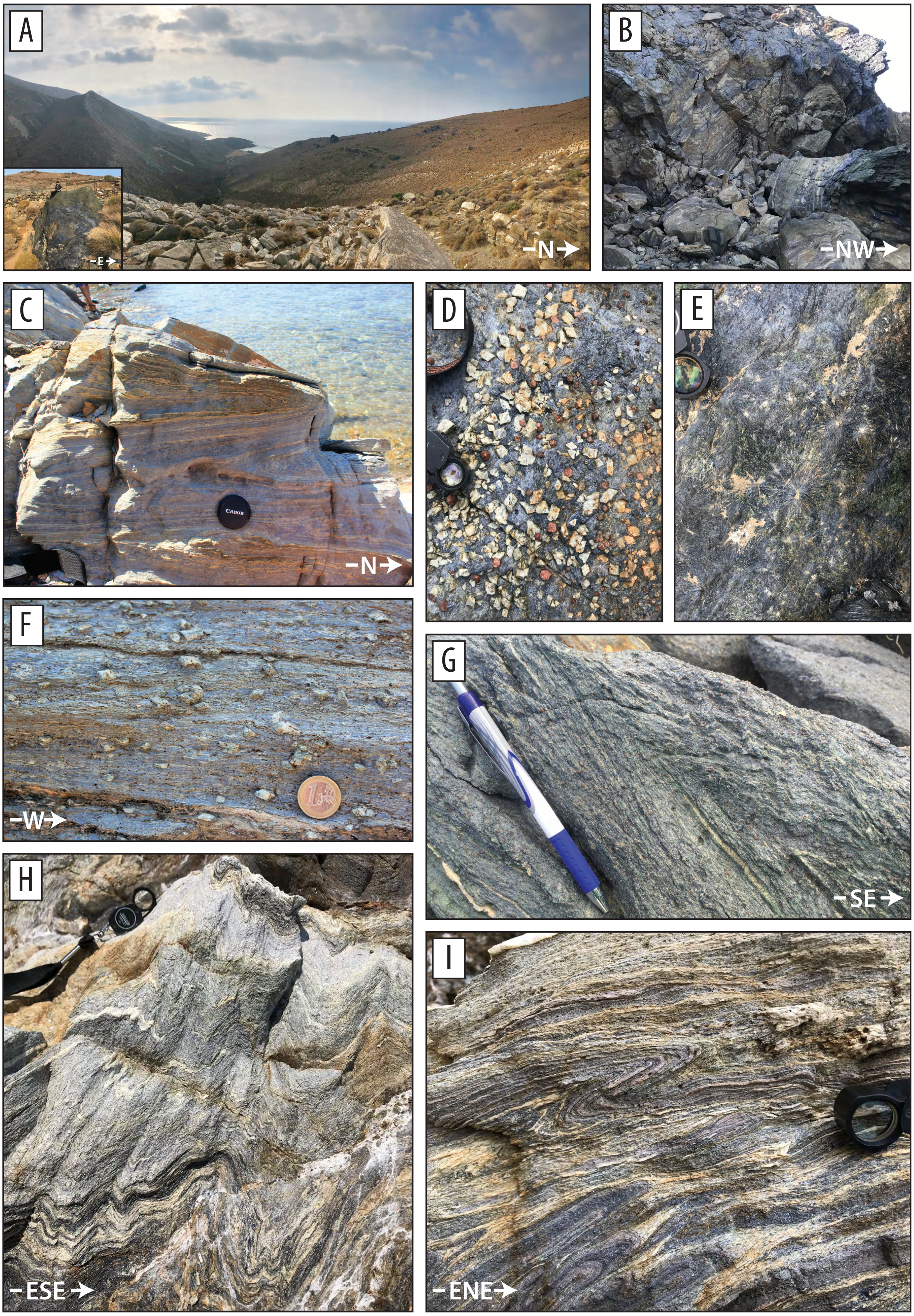

Figure C1: Caption to follow.

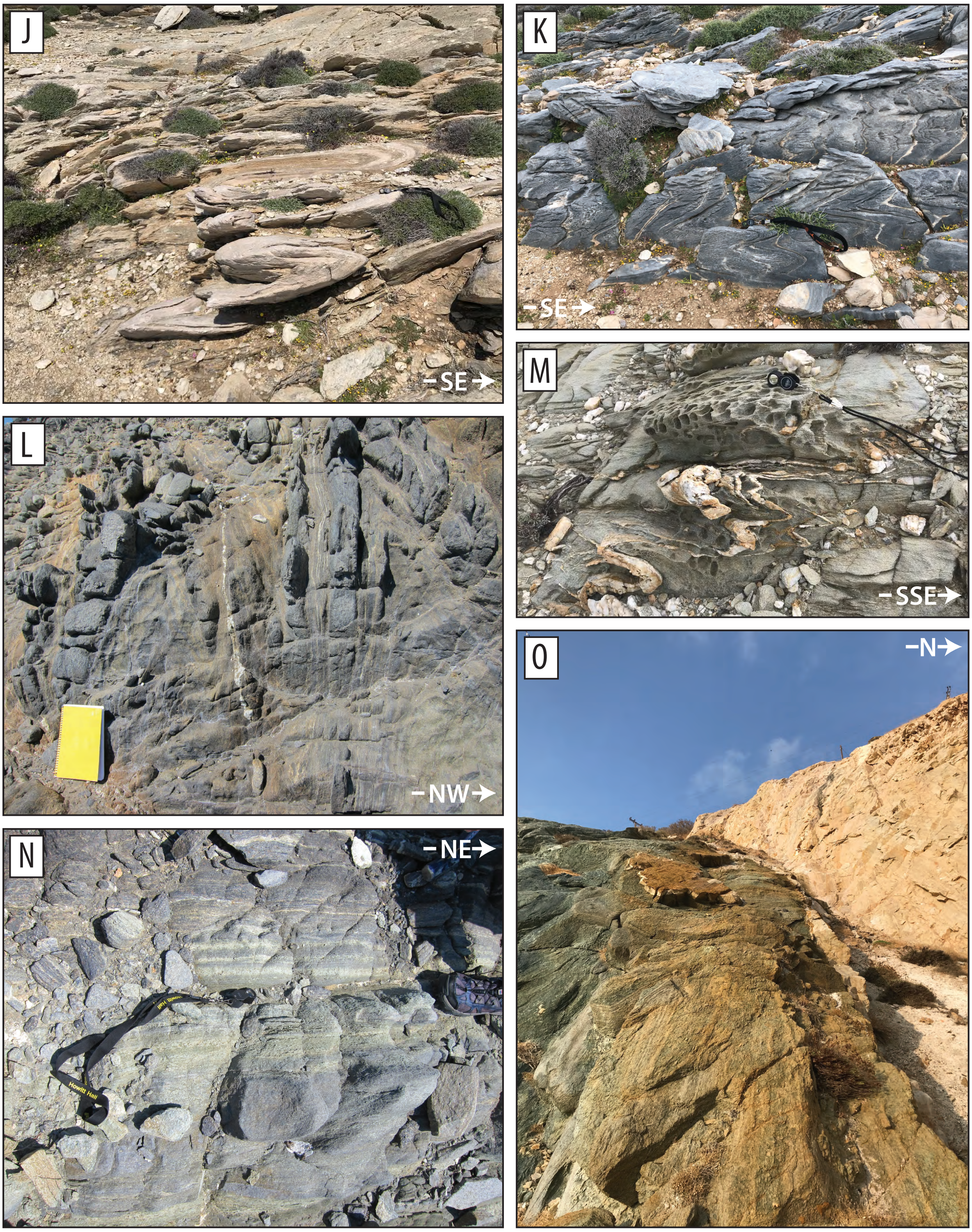

Figure C1: Caption to follow.

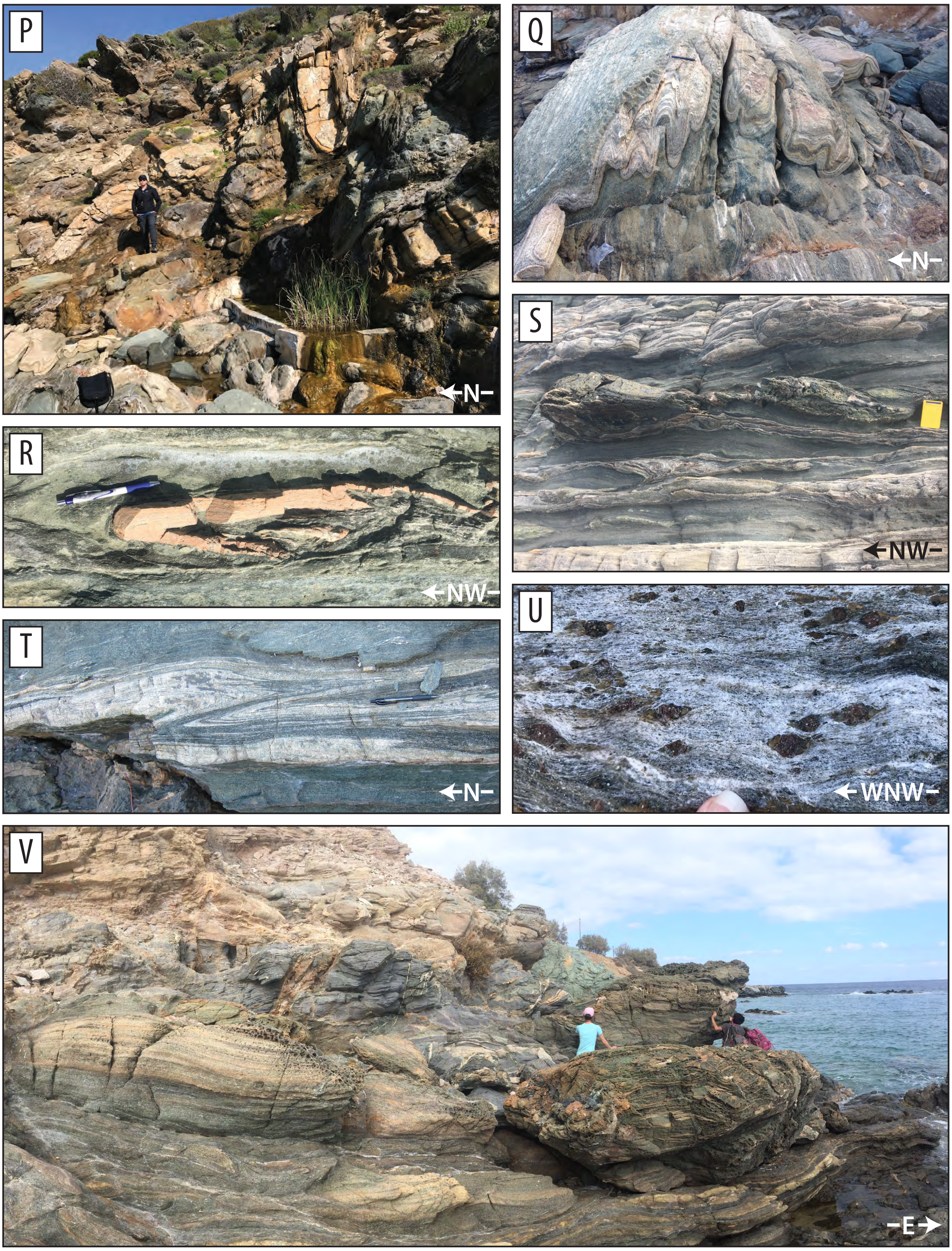

Figure C1: Caption next page.

Figure C1: (Previous pages.) Supplemental field photographs. (A) Eclogitic meta-gabbro 'blocks' pepper the Kampos Belt landscape, and are wrapped by coherent bimodal meta-volcanics (cropping out as resistant ledges in the background). Marbles in the foreground dip down towards the coastline and are structurally concordant with Belt rocks. This is a thrust contact that may have been reworked slightly during exhumation via extension, but we did not see evidence for strongly localized top-to-the-ENE shear. Inset shows example of Kampos meta-gabbro block with glaucophanite carapace. (B) Example of upright, shallowly NNE-plunging D_S folds on the shoreline W of Kampos Belt. (C) Lia Beach isoclinally-folded blueschists; the older, folded foliation is relict D_R, and isoclinal folding developed during D_S. (D) Unstrained cm-sized lawsonite pseudomorphs in Grizzas blueschist. (E) Zoom-in to margin of a Kampos Belt block showing static, radiating clusters of blue and green amphibole. (F) Unstrained D_S lawsonite pseudomorphs in Lia blueschists. (G) D_{T1} crenulation cross-cutting D_S at Kini. (H) The cores of D_{T1} upright folds in Azolimnos schists have strong axial planar cleavages associated with blueschist-to-greenschist facies retrogression. (I) Earlier D_S fabrics in Azolimnos schists record asymmetric shear in isoclinally-folded schists; pinkish layers are meta-cherts. (J) Isoclinal folds in marbles (foreground) and meta-conglomerates (background) and in meta-mafic greenschists (M) on Palos Peninsula mimic the map-scale folding seen in Fig. 2. (K) Sub-horizontal axial planar cleavages form in dolomitic blue-grey marbles during exhumation-related flattening (coaxial strain). (L) Upright D_{T1} folding at Kalamisia is associated with hinge-parallel greenschist retrogression (N) selectively permeating foliation-parallel layers. (O) Fault contact between marbles and blueschist-eclogite lithologies at Agios Dimitrios. Stretching is directly down-dip (essentially out of the page) and parallel to mullion hinges developed along the contact. Structures on either side of this contact are homogeneous. (P-S, U) Multiple generations of folding at Delfini. (P) Upright D_{T2} folding (discussed in text) develops an axial planar cleavage and hinge-parallel stretching and mineral lineations defined by quartz, epidote, and actinolite (Q). Older D_S foliations contain axial planes of isoclinal folds, best seen by salmon-colored meta-cherts (R) and compositional banding (T). Hinge:limb thickness variations locally exceed 20:1 (T, Lotos). (S) Along the limbs of upright folds like (P), coaxial stretching leads to boudinage of competent lenses. These structures record top-WNW shear, but top-ESE structures occur in roughly equal proportions. (U) Symmetric quartz-filled pressure shadows on delta-type D_S garnet porphyroblasts. (V) Asymmetric, non-coaxial strain during exhumation is limited to localities proximal to the Vari Detachment, like this example from Fabrikas.